Pflügers Arch – Eur J Physiol (2000) 439:403–415
Digital Object Identifier (DOI) 10.1007/s004249900135

ORIGINAL ARTICLE

A. Eke · P. Hermán · J.B. Bassingthwaighte
G.M. Raymond · D.B. Percival · M. Cannon · I. Balla
C. Ikrényi

Physiological time series: distinguishing fractal noises from motions

Received: 10 March 1999 / Received after revision: 29 June 1999 / Accepted: 26 July 1999 / Published online: 11 December 1999

Abstract Many physiological signals appear fractal, in having self-similarity over a large range of their power spectral densities. They are analogous to one of two classes of discretely sampled pure fractal time signals, fractional Gaussian noise (fGn) or fractional Brownian motion (fBm). The fGn series are the successive differences between elements of a fBm series; they are stationary and are completely characterized by two parameters, σ^2, the variance, and H, the Hurst coefficient. Such efficient characterization of physiological signals is valuable since H defines the autocorrelation and the fractal dimension of the time series. Estimation of H from Fourier analysis is inaccurate, so more robust methods are needed. Dispersional analysis (Disp) is good for noise signals while bridge detrended scaled windowed variance analysis (bdSWV) is good for motion signals. Signals whose slopes of their power spectral densities lie near the border between fGn and fBm are difficult to classify. A new method using signal summation conversion (SSC), wherein an fGn is converted to an fBm or an fBm to a summed fBm and bdSWV then applied, greatly improves the classification and the reliability of $\hat{H}$, the estimates of H, for the times series. Applying these methods to laser-Doppler blood cell perfusion signals obtained from the brain cortex of anesthetized rats gave $\hat{H}$ of 0.24±0.02 (SD, n=8) and defined the signal as a fractional Brownian motion. The implication is that the flow signal is the summation (motion) of a set of local velocities from neighboring vessels that are negatively correlated, as if induced by local resistance fluctuations.

Key words Brain microcirculation · Correlation · Fractal dimension · Fractals · Hurst coefficient · Laser-Doppler flowmetry · Temporal heterogeneity · Time series analysis

Abbreviations *bdSWV*: Bridge detrended scaled windowed variance method · β: spectral index · $\hat{\beta}$: estimate of spectral index · *Cov*: covariance · *d*: distance · *DHM*: the method of Davies and Harte, which produces the best known exact single fractal time series of the fractional Gaussian noise type · *Disp*: dispersional method · *f*: frequency estimate of the Fourier transform in a power spectral density function · *fBm*: fractional Brownian motion (motion for short) · *fGn*: fractional Gaussian noise (noise for short) · H: Hurst coefficient · $\hat{H}$: estimate of Hurst coefficient · $\hat{H}$': $\hat{H}$ calculated on summed signals by the bridge detrended scaled windowed variance method for the purpose of signal classification (the signal summation conversion method) · N: length of time series · *PSD*: power spectral density or periodogram method · *SSC*: signal summation conversion method for discriminating fGn from fBm signals · *SSM*: spectral synthesis method for generating fractal time series of fBm type · *SWV*: scaled windowed variance methods · τ: interval length · *Var*: variance

A. Eke (✉) · P. Hermán · I. Balla · C. Ikrényi
Experimental Research Department II. Institute of Physiology, Semmelweis University of Medicine, PO Box 448, 1446 Budapest, Hungary
e-mail: eke@elet2.sote.hu
Fax: +36-1334-3162

J.B. Bassingthwaighte · G.M. Raymond · M. Cannon
National Simulation Resource, Center for Bioengineering, University of Washington, Seattle, WA 98195–7962, USA

D.B. Percival
Applied Physics Laboratory, University of Washington Seattle, WA 98195–5640, USA

Introduction

Physiological signals are commonly irregular. The tendency is to regard such signals as random and to characterize them statistically by calculating their mean and standard deviation, as if assuming that the elements of the series are statistically independent of each other. This descriptive statistical approach is invalid, however, if the events are interdependent, having short- or long-range correlation. There is therefore a need to distinguish pure-

ly random noise from structured or correlated noise. Short-range correlation can be characterized by standard autoregressive moving average (ARMA) or ARIMA (I for integrated) techniques {[7] (see page 315), [12]}. Fractal methods are amongst those used to show long-range correlations [1, 4, 16, 37]. The methods of chaos analysis [4, 10, 15, 18, 33] are used to reveal underlying chaotic dynamics in low-order deterministic processes where the variation may appear similar to random but is in fact predictable.

Fractal methods can be applied to long memory processes with self-similar features. Self-similarity means that a feature has the same characteristic value independent of the scale at which the series is viewed, e.g., independent of the sampling rate of the observations. Basically one considers two kinds of fractal signals, fractional Gaussian noises, fGn, and fractional Brownian motions, fBm. fGn and fBm signals are interconvertible: when the elements of an fGn or noise signal are cumulatively summed, the resultant series is composed of the elements of a discrete fBm or motion signal; conversely, if one takes the differences between neighboring elements of an fBm signal one creates an fGn signal.

Each fractal analysis tool has different performance, prerequisite conditions, and limitations, and each needs thorough evaluation in order to avoid bias or misinterpretation of the derived fractal parameters [5, 6, 8, 9], especially when applied to physiological signals which may be contaminated with noise [15, 28]. The momentum of the newly emerging paradigm of fractal physiology [4] has created an upsurge in the application of fractal tools well before their thorough evaluation has been completed.

Often, a single analysis method, Fourier analysis, is applied to experimental data that might be either fGn or fBm, in order to estimate the fractal dimension. Because Fourier analysis is weak, often failing to distinguish fGn from fBm, and giving a rather imprecise estimate of the correlation structure [14], this is poor practice. Ideally therefore, a long memory process signal should be categorized as either stationary (fGn) or non-stationary (fBm) and the variance and correlation defined.

The final purpose of this study is to report measures of the fractal properties of high-resolution blood cell perfusion time series recorded by laser-Doppler flowmetry (LDF) from the rat brain cortex. Because of the peculiarly complex nature of this signal, we have had to develop new analysis techniques. The bulk of our presentation concerns the methodology, following the approach shown in Fig. 1, which will be further refined. Behind this general approach lie some details: (1) there are at least two kinds of fractal artificial time series, one being self-similar in its power spectral density and the other being self-similar in its long memory correlation; and (2) there are two well-characterized methods for estimating the Hurst coefficient (*H*), one for fGn (dispersional method or Disp) [6, 8] and one for fBm (bridge detrended scaled windowed variance method or bdSWV) [9], but none that is good for both.

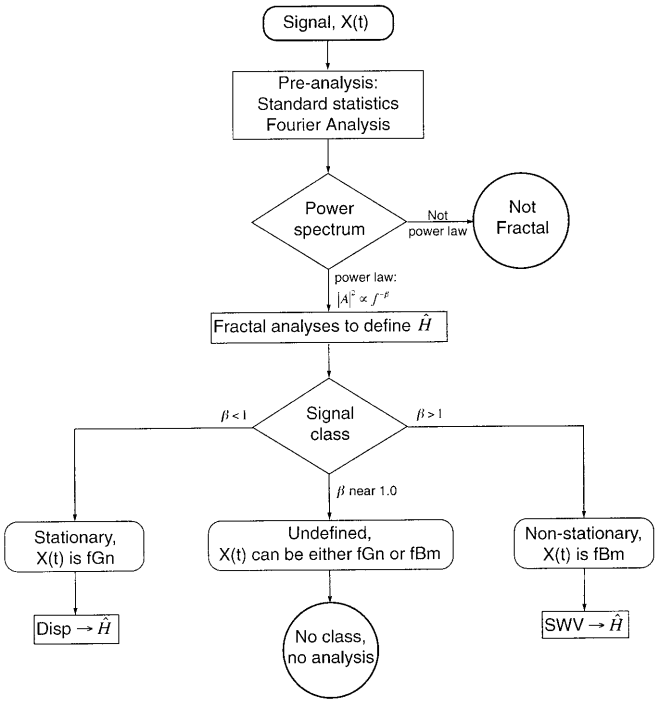

Fig. 1 General approach to the determination of fractal correlation structure (given by the estimated Hurst coefficient, $\hat{H}$) in time series. The fractal analysis is applied to series whose power spectral density functions (*PDF*, from Fourier analysis) mimic a power law, $|A|^2$=f. This study focuses on estimating $\hat{H}$ as accurately as possible, having signal class determined by stationary/non-stationary categories. This approach minimizes the range of β near the critical boundary of 1.0, where signals cannot be classified and hence analyzed. (*Disp.* dispersional analysis, *fGn* fractional Gaussian noise, *fBm* fractional Brownian motion, *SWV* scaled windowed variance analysis)

The strategy (Fig. 1) is therefore to put together the information gathered from a coherent set of analyses to give the best characterization. This starts with a "pre-analysis" using standard statistics and Fourier analysis, as in the upper part of the diagram, and is followed by a decision based on the form of the Fourier power spectral density, PSD. If the PSD has a clear power law form over an adequate scaling range (preferably a 100-fold range of frequencies) then fractal analysis is undertaken. If the signal $X(t)$ is clearly an fGn then Disp is used as the primary method for estimating H, and if the signal is clearly an fBm the bdSWV is used. The working definitions of what "clearly" means are taken from the evaluation of the signal characterization methods with respect to their accuracy, for a signal of a given length, on each of the two types of pure artificially generated fractal signals. The end result is a detailed refinement of the strategy shown in Fig. 1, and the use of that strategy in characterizing the complex signal obtained by LDF from the rat cerebral cortex.

Background principles for the methods

Fractals and time series

A time series is defined as a discrete series, X_i for i=1,…,N, and is a sampled representation of a temporal process or signal, $X(t)$ sampled at equal intervals in time, Δt. Preliminary analysis (Fig. 1) of signals involves estimating the mean value, standard deviation and skewness. ARMA and ARIMA are traditionally used by statisticians to estimate short-range correlation. Fourier analysis reveals the signal's content of relative power versus frequency, and is an essential guide to deeper analysis. One can use Fourier analysis also to provide estimates of the short-range correlation between elements of the series.

Fractal processes are long memory processes with self-similarity

Fractals develop in space or time by the operation of a process resulting in objects or events characterized by self-similarity [22], which refers to the apparent geometrical or statistical similarity between elements of the object or event independent of the scale of observation. A geometrical fractal can be divided into Z smaller copies of itself, each of which is scaled down by a factor r. When the scaling superimposes the longer upon the smaller version, the object is "self-similar" and $\log(Z)/\log(1/r)$ is a measure of the fractal dimension D [36]. For one-dimensional time series, D is greater than 1, indicating that the signal has variability or roughness. H=2–D [19] and is a measure of a scale-independent structural property, in visual terms the "roughness" of the signal. H near 1.0 indicates a high degree of smoothness or close correlation, H near 0 indicates a high degree of roughness, actually anticorrelation (Fig. 2). An H of 0.5 indicates the absence of correlation, i.e., uncorrelated or white noise.

Self-similarity

Three basic features of fractal signals are self-similar. The first is the appearance. If an fGn is observed at scale $1/r$ and its amplitude is rescaled by r^H, $X(rt)$ is seen to look like the original $X(t)$ and is statistically indistinguishable from it. [If $X(t)$ is an fBm then the self-similarity is in the successive differences.] Formally, since the units of X_i are not time, the series is defined as being self-affine rather than self-similar. The second is reflect-

Fig. 2 Relationship between exact single fractal time series generated according to the dichotomous fGn/fBm model of random signals and its fractal descriptors, H and β (*left*). Spectra of selected time series shown in the *middle* with regression slope fitted to obtain $\hat{\beta}$. On the *right*, idealized spectral slopes are shown for different ranges of the fGn/fBm model along with landmark values of β and r_1. Special cases are *rn* (random noise) and *rw* (random walk signals). (*PSD* Power spectral density)

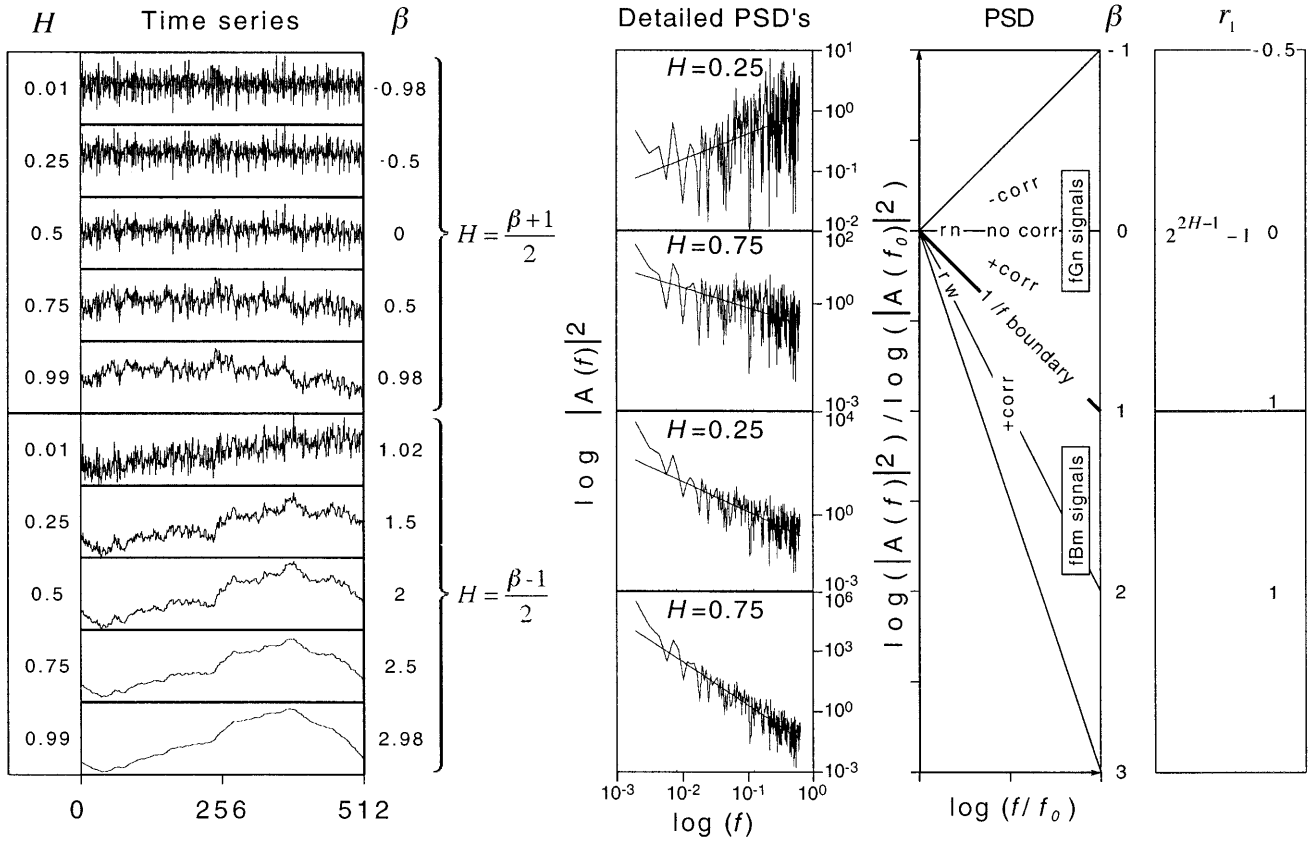

ed in its Fourier power-spectrum (Fig. 2, second and third panels): the power–law relationship expresses the idea that as one doubles the frequency the power diminishes by the same fraction regardless of the chosen frequency, i.e., the ratio is independent of where one is on the frequency scale. The power versus frequency relationship is:

$$|A(f)|^2 \propto c \cdot f^{-\beta} \tag{1}$$

where c is a constant, A is the amplitude of the Fast Fourier Transform (FFT) at a given frequency f and β is the spectral index or exponent. On a log–log plot Eq. 1 gives a straight line with slope $-\beta$.

Fractal signals with $-1<\beta<1$ are fGn's; they have constant variance at all times, which classifies them as *stationary* signals (Fig. 2). Those with $1<\beta<3$ are non-stationary because their observed variances increase with t, the length of the observation period, such that $\mathrm{var}[X(t)] \propto t^{2H}$ [7, 24]. The PSD function of an fBm series has a slope β that is 2 less than that for the original fGn series, at least for the low frequencies (Fig. 2). Noises and motions of the same H thus have β values that differ by 2. (This statement does not apply to the highest frequencies, specifically for the range of $1/2^3<f<1/2^1$, where the PSD is deformed by summing or differencing [7]. Here we define f as actual frequency divided by the sampling frequency.)

The third self-similar feature is the autocorrelation. In the range of non-integer spectral indices fGn signals show either correlated or anticorrelated structuring, while near neighbor elements of a motion signal are positively correlated for all H. Even though the expected mean value $E[(t)]=0$ for all t, correlation between elements of a non-stationary fBm signal, $X(t)$ and $X(t+\tau)$, is time dependent just as variance, $\mathrm{var}[X(t)]$, is time dependent and increases to infinity as t goes to infinity [7]. The correlation r_τ is given as:

$$r_\tau = \frac{\mathrm{covariance}\{X(\tau), X(t+\tau)\}}{\mathrm{variance}\{X(t)\}} = \frac{\Sigma\{X(\tau)\cdot X(t+\tau)\}}{\sqrt{\{X(t)\}\cdot\{X(t+\tau)\}}} \tag{2}$$

For motion signals, fBm, the value of r_τ depends on both t and τ. For any fixed τ, r_τ approaches 1 as t approaches infinity for all H. A noise signal, an fGn process, is stationary and has a time-independent correlation structure, i.e., $[X(t),X(t+\tau)]$ depends only on τ and H, since $\mathrm{var}[X(t)]$ is constant, and the correlation coefficients [3, 7, 24, 35], r_τ are:

$$r_\tau = \frac{1}{2}\{|\tau-1|^{2H} - 2|\tau|^{2H} + |\tau+1|^{2H}\} \tag{3}$$

Time series adhering strictly to Eq. 3 are called exact fractals. These give the power law behavior at low frequencies but deviate from Eq. 1 at high frequencies. For the nearest neighbors, X_i and X_{i+1}, or $\tau=1$ the correlation [35] is:

$$r_1 = 2^{2H-1} - 1 \tag{4}$$

Table 1 Naming conventions

Convention	Description
${}^{\text{operator}}_{\text{generator}}H^{\text{signal}}_{\text{analysis}}$	Usage of indices for referring to different aspects of fractal analysis associated with the assessment of *H*: *generator* = method producing a time series (DHM or SSM); *operator* = operation performed on the time series prior to fractal analysis: *none*, or *s* = summed, or *d* = differenced; *signal* = series type: *fGn* or *fBm*; *analysis* = method of fractal analysis, (Disp, bdSWV, PSD's)
${}^{\text{low}}\text{PSD}_{\text{w,e}}$	Variant of the PSD method using the following operations: *w* = applying parabolic windowing, *e* = endmatching, *low* = excluding the high-frequency spectral estimates ($1/8<f<1/2$) when obtaining $\hat{\beta}$ by fitting for the slope of regression

The first lagged autocorrelation may be positive, zero or negative. White or random noise (shown by the third row of the left panel of Fig. 2 and marked as rn in the third column panel of Fig. 2) is the fGn signal with all the frequencies represented at equal power and no correlation between adjacent elements with $\beta=0$, $r_1=0$ and $H=0.5$. A random walk is the cumulative sum of this particular fGn and is the fBm signal marked as *rw* with $\beta=2$, $r_1\rightarrow 1$ in the third and fourth panels of Fig. 2. The self-similarity in the autocorrelation function is such that if nearest neighbors are positively correlated this correlation extends over infinite time and falls off with τ in a self-similar fashion [3, 4]:

$$\frac{r(\tau_1)}{r(\tau_2)} = \left(\frac{\tau_1}{\tau_2}\right)^{2H-2} \tag{5}$$

Thus $r(\tau)$ also diminishes as a power law function of the distance τ between a pair of elements. Using the fractal methods, which follow, gives more accurate estimates than Fourier methods can of $r(\tau)$ from fGn and fBm. In fractal methods all of the data are used to determine one value, H, representing a set of scaled $r(\tau)$ values; Fourier methods give a set of $N/2$ independent values of $r(\tau)$ for a series of N elements.

Naming conventions are given in Table 1.

Methods

Methods of analysis

Power spectral density (PSD or periodogram) analysis

The power spectral amplitude function, shown in Fig. 2, $|A(f)|^2$, was estimated from X(t) by the FFT algorithm (periodogram [32]) providing the estimated power $|A(f)|^2$ at frequencies increasing by a factor of 2^p, where p is a positive integer. (For series whose length is not exactly 2^p, to use the efficient FFT algorithm, the series may be extended to length 2^p by adding zeroes to the end of the series, called "zero padding". While this shifts the apparent fundamental frequency, it does not distort the spectrum.) H was estimated from a log–log plot of the periodogram fitting a straight line of slope $-\beta$ [31, 36]. The standard periodogram should be re-

served for estimation when $\beta \leq 2$. For $\beta > 2$ Fougere [14] recommended end matching (e) or bridge detrending [9] of the fBm signals; this is done by subtracting from the data the line connecting the first and last points of the series and applying a parabolic window (w) before analysis. The parabolic window for a series of length N is a function that multiplies each value in the series and is given by:

$$W(j) = 1 - \left(\frac{2j}{N+1} - 1\right)^2 \quad \text{for } j = 1,..., N. \tag{6}$$

Removal of the series' mean improves the consistency of spectral estimates for fBm signals but has no effect on fGn signals. The mean was subtracted from all series evaluated in this study. Combinations of these procedures have been tested in numerical experiments. In disagreement with Fougere, we found that parabolic windowing should precede the step of end matching, and that high-frequency power estimates need to be excluded when fitting for β, a method we designate ${}^{low}PSD_{we}$.

Dispersional analysis (Disp)

This statistical approach using relative dispersion, introduced by Bassingthwaighte [1], is applicable only to fGn signals. It is based on the variability of the local averages of the signal over windows of length $\tau = n \cdot \Delta t$. It uses standard deviation, SD, of these local averages, and repeats the calculation for many different τ values. H equals 1 plus the slope of the regression of log [SD(τ)/SD(τ_0)] versus log [τ/τ_0], where τ_0 is a reference window size

$$\log \mathrm{SD}(\tau) = (H-1)\log\left(\frac{\tau}{\tau_0}\right) + \log \mathrm{SD}(\tau_0) \tag{7a}$$

or

$$\mathrm{SD}(\tau) = \mathrm{SD}(\tau_0)\left(\frac{\tau}{\tau_0}\right)^H \tag{7b}$$

Scaled windowed variance (SWV) analyses

These methods, applicable only to fBm signals, divide a series into non-overlapping windows of size $\tau = n \cdot \Delta t$, compute a measure of variability (standard deviation, SD) in each of these windows, and then find the average SD(τ) for that window size. One then repeats the computation for windows of a wide range of τ. The bridge detrended scaled windowed variance method, bdSWV [9], is a variation introduced by Mandelbrot [23] and developed further by Peng et al. [26]. It was used in this analysis in an attempt to reduce the bias in the H estimated from the standard method [31, 34]. The slope of log [SD(τ)/SD(τ_0)] versus log [τ/τ_0] is the estimate of H, $\hat{H}$:

$$\log \mathrm{SD}(\tau) = H\log\left(\frac{\tau}{\tau_0}\right) + \log \mathrm{SD}(\tau_0) \tag{8a}$$

or, showing H as exponent:

$$\mathrm{SD}(\tau) = \mathrm{SD}(\tau_0)\left(\frac{\tau}{\tau_0}\right)^H \tag{8b}$$

Signal summation conversion method

The signal summation conversion (SSC) method is used to refine the analysis of signals for which β is near 1, as diagrammed in Fig. 1. There are two steps: (1) calculate from X_t its cumulative sum (this converts an fGn to an fBm or converts an fBm to its cumulant), and (2) use the bdSWV method to calculate from the cumulant series a Hurst coefficient $\hat{H}$'. The interpretation of $\hat{H}$' is that when $0 < \hat{H}' = < 1$, then X_t is an fGn with $\hat{H} = \hat{H}'$. Alternatively when $\hat{H}' > 1$, then the cumulant series is identified as an fBm signal with $\hat{H} = \hat{H}' - 1$ and then the bdSWV method directly applied to the original X_t gives the best estimate of $\hat{H}$.

Generating precisely known fGn and fBm series to test analysis methods

Signals of known H were generated by two methods: the Davies and Harte method (DHM) for generating fGn signals with correlation exactly as given by Eq. 3 [8, 11], and the spectral synthesis method (SSM) [2, 5, 6, 11, 29, 30] producing fBm signals with the power law behavior of Eq. 1. For the DHM-generated fGn the power spectrum fails to follow the power law of Eq. 1 at high frequencies [7]. For the SSM signal the autocorrelation tends to zero at the high frequencies. Both are fractals, but with respect to different properties. Signals generated by DHM were converted to fBm by summation and SSM-generated signals (fBm) were converted to fGn by differencing.

Signals were generated by each method for series length $N = 2^{17}$ for $0.01 \leq H \leq 0.09$, and $0.91 \leq H \leq 0.99$ in steps of $\Delta H = 0.01$, for $0.1 \leq H \leq 0.09$ in steps of $\Delta H = 0.1$, 100 series for each of 27 values of H. An additional 2700 series were generated by either differencing or summing to provide the associated fGn or fBm.

Numerical experiments to evaluate the reliability of fractal methods

The fractal analytical methods were tested on synthesized fractal signals of known H in the style used previously [5, 6, 8, 9, 30], to obtain from each an estimate of H. For each set of series of known H and particular N the variance and bias were calculated. The mean squared error (MSE=var+bias^2) was used to give a combined characterization of bias and variance in $\hat{H}$. Methods were rank ordered according to their MSE, and their overall performance was judged based on their ranked position. Length N was chosen to be 2^{17}, or 131,072 elements, which is long enough for the estimates of H to have a small variance [5, 6].

Numerical experiments to test signal classification methods

Two methods were tested: ${}^{low}PSD_{w,e}$ as the most reliable variant of the PSD methods, and our signal summation conversion method (SSC). As seen in Fig. 2, the special case of spectral slope $\beta = 1$ separates fractal noise from fractal motion. Hence signal classification methods should be tested, based on their estimates of the spectral slope $\hat{\beta}$, on synthetic fractal signals of known β. Hence100 single fractal signals of known β were generated at a signal length of 2^{17} by the DHM method for each value of β in steps of 0.02 for $-0.98 \leq \beta \leq 0.98$, and $1.02 \leq \beta \leq 2.98$. The modified power spectral density method ${}^{low}PSD_{w,e}$ yields β directly, while our SSC method yields $\hat{H}$' from which $\hat{\beta}$ can be calculated as $\hat{\beta}$. The reliability of these methods in distinguishing fractal noises from motions was characterized by computing the misclassification rate of faulty decisions on $\hat{\beta}$.

Testing the applicability of fractal tools to physiological data

We chose as examplary data sets the signals from LDF from the microcirculation of the outer 2 mm of the gray matter of the left parietal cortex of the rat brain [13]. These signals are a composite of individual blood cell velocities (predominantly that of red blood cells) in the catchment volume of the probe. The signals appear noisy (upper panel, Fig. 3), but the goal is to test for fractal correlation structure, which would identify the signal as different from random noise.

The signals were from male Wistar rats (n=8, body weight= 290±35 g) anesthetized by Urethane (130 mg/100 g body weight intraperitoneal), and artificially ventilated by a gas mixture of 30% O_2 and 70% N_2. These signals were acquired in the control period of a complex study aimed at analysis of LDF signal fluctuations under normal conditions and during controlled arterial hypotension (not reported herein). Since the hypotension was induced by lower body pooling of circulating blood by placing the animal in a suction device, the right carotid artery was cannulated

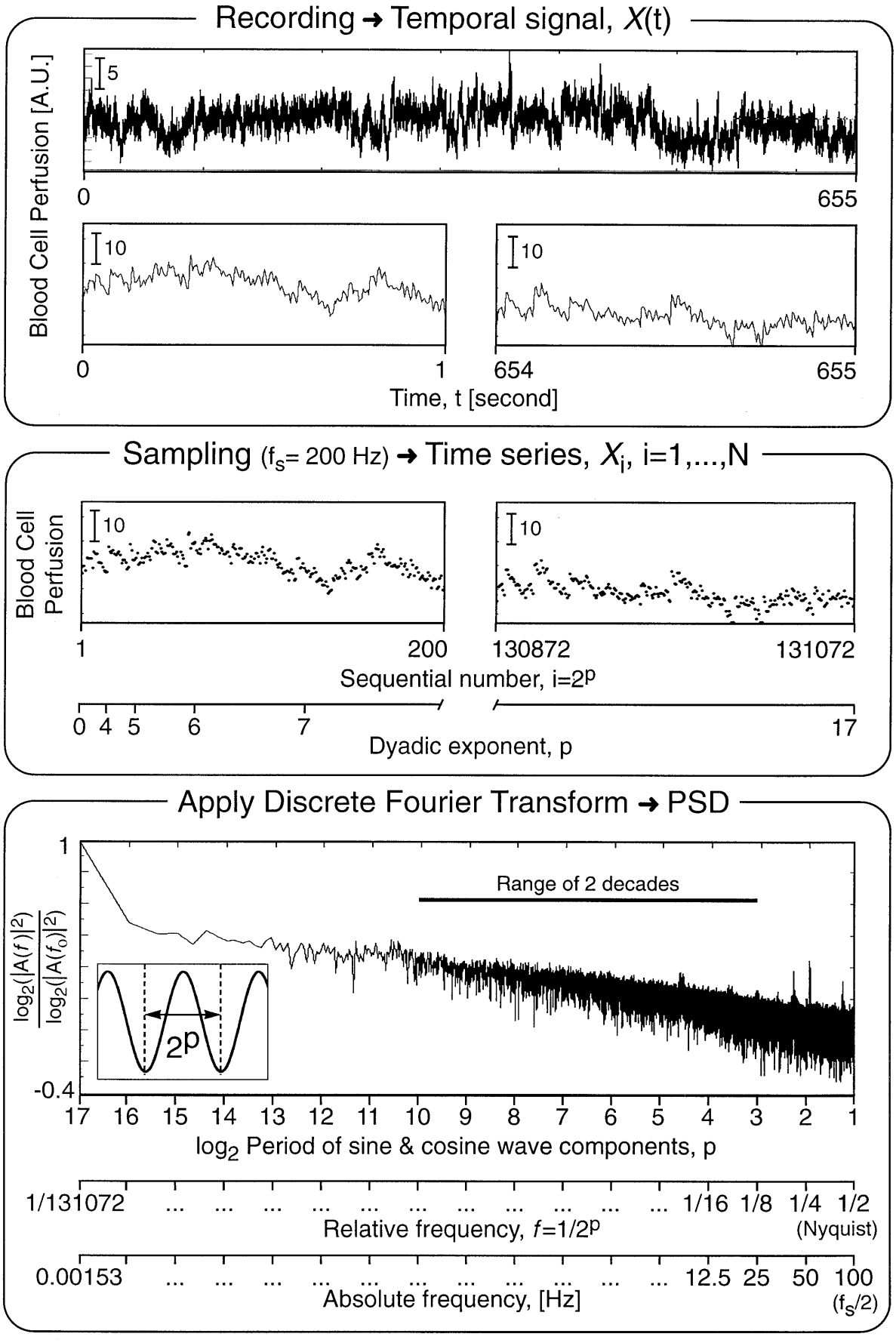
Recording ➜ Temporal signal, X(t)
Blood Cell Perfusion [A.U.]
5
0
655
10
0
1
10
654
655
Time, t [second]
Sampling (fs= 200 Hz) ➜ Time series, Xi, i=1,...,N
Blood Cell Perfusion
10
1
200
10
130872
131072
Sequential number, i=2p
0 4 5 6 7
17
Dyadic exponent, p
Apply Discrete Fourier Transform ➜ PSD
1
-0.4
Range of 2 decades
log2(|A(f)|2) / log2(|A(fo)|2)
2p
17 16 15 14 13 12 11 10 9 8 7 6 5 4 3 2 1
log2 Period of sine & cosine wave components, p
1/131072 ... 1/16 1/8 1/4 1/2
Relative frequency, f=1/2p
(Nyquist)
0.00153 ... 12.5 25 50 100
Absolute frequency, [Hz]
(fs/2)

Table 2 Results of fractal analysis of blood cell perfusion time series. Data are shown for the two major phases of the analysis, namely signal classification and calculation of Hurst coefficients

Series	Spectral classification by $^{low}PSD_{w,e}$		SSC classification			Hurst coefficients		
	$\hat{\beta}$	Signal class	$\hat{H}$'	$\hat{\beta}$	Signal class	$\hat{H}_{PSD}$	$\hat{H}_{bdSWW}$	$\hat{H}^{fBm}$
ts.1	1.51	fBm	1.35	1.55	fBm	0.25	0.27	0.26
ts.2	1.45	fBm	1.12	1.46	fBm	0.22	0.23	0.23
ts.3	1.41	fBm	1.04	1.44	fBm	0.20	0.22	0.21
ts.4	1.44	fBm	1.10	1.43	fBm	0.22	0.21	0.22
ts.5	1.53	fBm	1.16	1.51	fBm	0.26	0.25	0.26
ts.6	1.53	fBm	1.19	1.48	fBm	0.27	0.24	0.25
ts.7	1.47	fBm	1.17	1.44	fBm	0.23	0.22	0.23
ts.8	1.50	fBm	1.15	1.48	fBm	0.25	0.24	0.24

for perfusion pressure. In a series of tests, in agreement with observations of others and in accord with expectations since the vertebral arteries are large, we demonstrated that, following a transient drop, the LDF signal returns to the precannulation level. The LDF signals, blood cell perfusion versus time, were recorded using a Moor Instruments, MBF3D, with a time constant of 0.1 s in control conditions over the left parietal region through the thinned, intact calvarium [13]. The blood cell perfusion signal was digitized by a PCL 711 Advantech Lab Card installed in an IBM 486 DX50 computer at 200 Hz at 12 bit. Blood cell perfusion time series were created from the sampled records, 131,072 (2^{17}) data points in length, representing a record of 655 s each at an equal increment Δt of 0.005 s [13].

Results

Blood cell perfusion in the rat brain cortex

High-resolution blood cell perfusion signals such as those shown in Fig. 3 were obtained from eight rats, with a total signal length, N, of 2^{17} for each. All animals were in steady state as judged by steady and normal levels of body temperature, mean arterial blood pressure, and blood gases. The mean blood cell perfusion levels were around 250 units for these animals and the standard deviations were 1% of the mean (Table 2). Fourier analysis provided PSD functions, similar to that shown in Fig. 3 (which is for rat number 6). The PSD has the appearance of a power law relationship as prescribed for a single fractal by Eq. 1.

Fig. 3 Steps of time series analysis by the Fourier method of a blood cell perfusion signal recorded from the brain cortex of an anesthetized rat. A continuous 655-s record with a mean of 238.8 relative units is shown at the *top* (this is for animal 6 labeled as *ts.6* in Table 2). *Middle*: discrete sampling at a frequency, f_s=200Hz, yields the time series X_i, whose first and last second segments are shown. *Bottom*: the PSD plot is shown. The *ordinate* is the power at any given frequency normalized by the power at the lowest relative frequency component ($f_0=2^{17}$). The operation (Discrete Fourier Transform) leading to a PSD plot is based on obtaining the Fourier series for sine and cosine waves of period 2^p (see *inset*), from which at the given frequency, $1/2^p$, the power is calculated. By the inversion of this operation (Inverse Fourier Transform) the original signal can be reconstructed from its sine and cosine wave components. The *abscissa* of the PSD plot can be expressed in either the period of the sine and cosine wave components, p, the relative, $1/2^p$, or the absolute frequency $f_s/2$. The highest frequency in a PSD plot is half of f_s and is called the Nyquist frequency. Fractal analysis utilizing the Fourier method is based on a linear fit of the power spectral estimates of the log–log PSD plot for its estimated spectral index $\hat{\beta}$. Fractal analysis can be undertaken if the power law relationship between power estimates and frequency prescribed by Eq. 1 is present in a range larger than two decades (shown by the *bar*)

Precision of fractal tools in estimating H from the known signals

The estimate, $\hat{H}$, exhibited biases and variance depending on the method itself ($^{low}PSD_{w,e}$, Disp, and bdSWV), the type of the signal analyzed (fGn versus fBm), and the signal generating process (DHM and SSM). In each panel of Fig. 4 the estimates, $\hat{H}$, are plotted as the mean from each 100 series of length 2^{17} for each H. The three columns show the results obtained by three analysis methods: $^{low}PSD_{w,e}$, Disp, and bdSWV, a total of 3300 estimates. The top two rows are signals generated by the exact correlation method, DHM, the top row being fGn, and the second row being the fBm formed by summation. The bottom two rows give the SSM signals.

Spectral slopes

Tested on fGn generated by DHM, $^{low}PSD_{w,e}$ showed some bias below H=0.3 with a steep increase below H=0.1 (Fig. 4 A1, A2). This same analysis method gave zero bias on SSM signals (Fig. 4 A3, A4), which is because the signal generation and analysis are both based on Eq. 1.

Variance analysis

Disp (Fig. 4 B1) and bdSWV (Fig. 4 C2) are highly reliable and have low bias in estimating H when evaluated on DHM-generated fGn or the cumulant fBm signals. The MSE of 0.00006 and 0.00056, respectively, are one and two magnitudes better than the 0.01 of $^{low}PSD_{w,e}$. These same methods did less well but adequately on SSM signals (Fig. 4 B3, C4). The combination of these

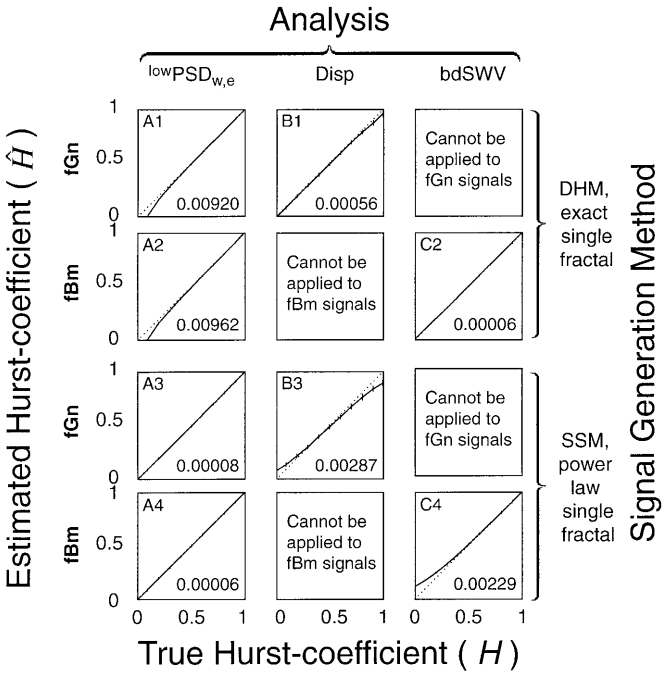

Fig. 4 Accuracy (deviation from the dotted line of identity) and precision (indicated by vertical bars of ±1SD) of estimates, $\hat{H}$, of the Hurst coefficient (*ordinate*) from single fractal signals of known H (*abscissa*) generated by the method of Davies and Harte [11] (*DHM*), and the spectral synthesis method (*SSM*). Signals of length $N=2^{17}$ were evaluated: power spectral density (*PSD*), dispersional (*Disp*), and bridge detrended scaled windowed variance (*bdSWV*) methods. The PSD method was implemented using a combination of pre-processing operations: parabolic windowing (*w*), endmatching (*e*), using only spectral estimates up to $f=1/8f_s$ (low). H was varied in increments of 0.1 in between 0.1 and 0.9 in addition to being set to 0.01 and 0.99. The mean $\hat{H}$ and SD were obtained in 100 realizations. Mean squared error, *MSE*, for the 1100 points on each panel *is* calculated as $\mathrm{MSE}=\sum_{i=1}^{11}\left[\left(\text{average}\hat{H}-H_i\right)^2+\mathrm{SD}_i^2\right]$ where the subscript *i* indicates a series of100 runs. MSE is shown in the *lower right corner* of each plot. Plots are also identified in the *upper left corner* by their *column* and *row position*

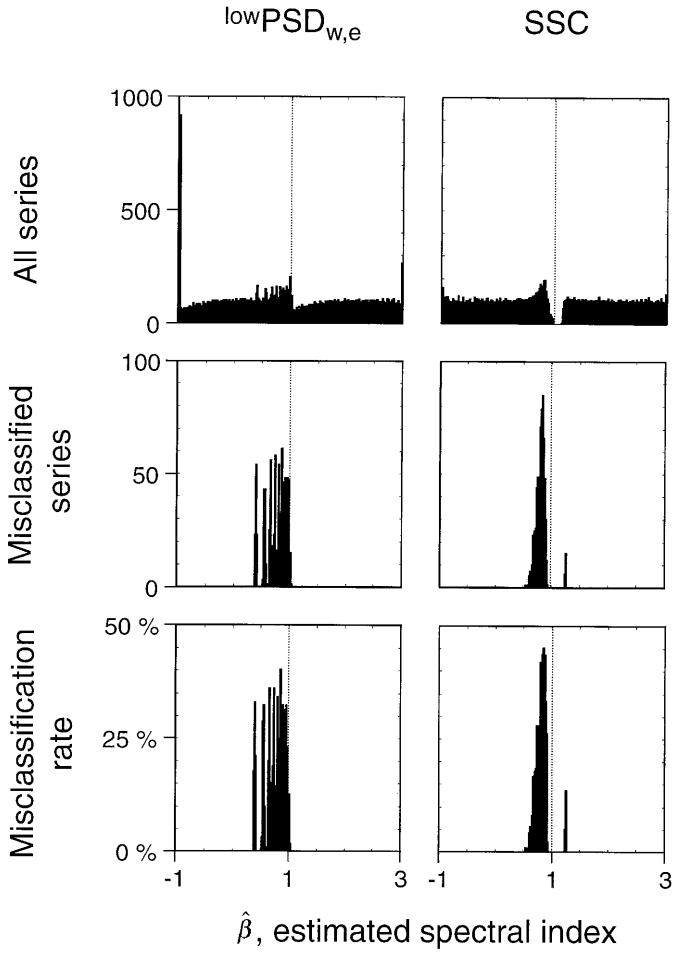

Fig. 5 Characterization of the precision of signal classification by the best overall Fourier method, $^{low}PSD_{w,e}$, and our signal summation conversion (*SSC*) method. *Dotted lines* at $\hat{\beta}=1$ mark the boundary separating fGn from fBm signal categories. The histograms were generated using a bin size of 0.02. β was estimated by the two methods in 5400 realizations on DHM-generated exact single fractal signals. *Top*: frequency distribution of $\hat{\beta}$. Cases evaluated by $^{low}PSD_{w,e}$ with $\hat{\beta}>3$ are plotted together with cases in the outermost bins of $-1<\hat{\beta}<-0.98$ and $2.98<\hat{\beta}<3$, respectively. While $\hat{\beta}$ of the $^{low}PSD_{w,e}$ column was estimated by one, that of the SSC column by two methods depending on the signal class found by $\hat{H}$', as $\hat{\beta}^{fBm}=2\hat{H}_{bdSWV}+1$ or as $\hat{\beta}^{fGn}=2\hat{H}_{Disp}-1$. *Middle*: histograms created from cases, when the class corresponding to $\hat{\beta}$ turned out to be different from the expected class based on β at which the signal was generated. For example, when a signal generated at $\beta=1.2$ (an fBm) was classified as fGn with $\hat{\beta}=0.98$, an entry to this histogram was made at $\hat{\beta}=0.98$. *Bottom*: histograms of misclassification rate calculated as percentage of misclassified cases (*middle*) relative to the total falling in a particular bin based on $\hat{\beta}$ (*top*). Note that no signals were generated for $\beta=1$ being an undefined condition for the DHM method

two robust methods, Disp and bdSWV, provides the best basis for estimating H from random signals from the fGn/fBm models.

Precision of signal classification methods

Since our analysis of physiological signals is based on the fGn/fBm dichotomy, classification of the signal as fGn or fBm is a central goal. We tested the PSD method on DHM-generated signals, both fGn and fBm. The top panels of Fig. 5 show the total number of estimates at a given β; if all were exactly correct there would be 100 estimates at each H, but both power spectral analysis and the SSC give errors. The PSD method gives a lot of estimated values of β near zero and also shifts some of those fBm signals with $\beta>1$ to values <1 (left middle, Fig. 5). Inside the range $0.38<\beta<1.04$ there was about 40% uncertainty in defining the signal class by $^{low}PSD_{w,e}$. Our SSC approach also has error when β is near 1.0 (right middle, Fig. 5), but narrows the range in which fGn cannot be distinguished from fBm (ranges of misclassification rates shown in the bottom panels).

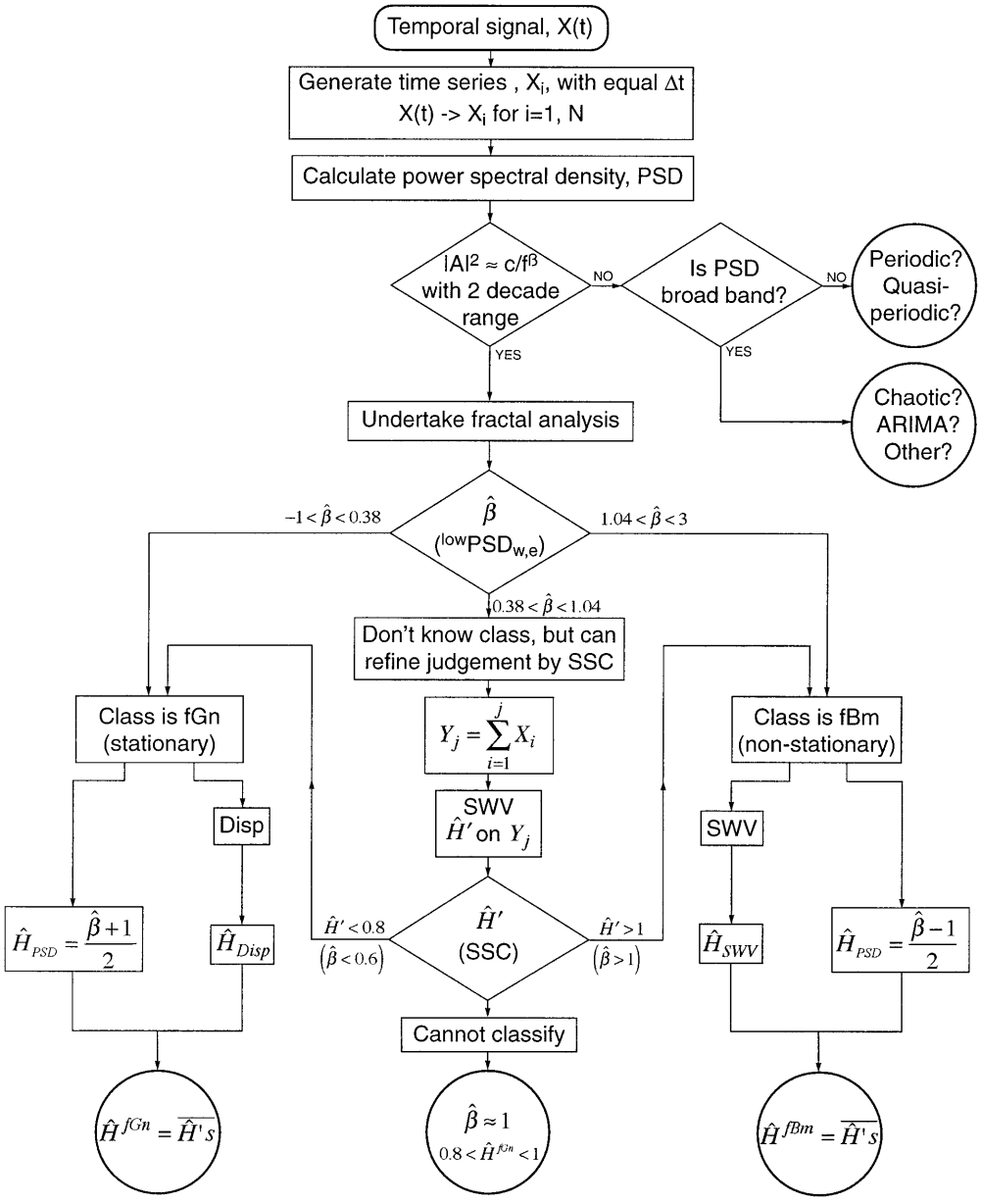

Fig. 6 Flowchart for fractal analysis. The system is hierarchical and dichotomous, in that each step provides a conclusion on one aspect of the analysis, a prerequisite to proceed, such as "is scaling range larger than two decades", or "is signal of fGn or fBm type". Conditions to be tested are given in *diamonds*. Possible endpoints of the analysis are displayed in *circled frames*. [*bdSWV* Bridge detrended scaled windowed variance analysis, β spectral index, $\hat{\beta}$ estimate of spectral index, *Disp* dispersional analysis, *f* frequency estimate of the Fourier transform in a power spectral density function, *fBm* fractional Brownian motion, *fGn* fractional Gaussian noise, *H* the Hurst coefficient, $\hat{H}$, the estimates of *H*, for the times series, $\hat{H}'$: $\hat{H}$ calculated on summed signals by the bridge detrended scaled windowed variance method for the purpose of signal classification (the signal summation conversion method), *N* length of time series, *PSD* power spectral density or periodogram method, *SSC* signal summation conversion method for discriminating fGn from fBm signals, *SSM* spectral synthesis method for generating fractal time series of fBm type, *SWV* scaled windowed variance methods.] $^{low}PSD_{w,e}$ is a variant of the PSD method using the following operations: *w*, applying parabolic windowing; *e*, end-matching; *low*, excluding the high-frequency spectral estimates ($1/8<f<1/2$) when obtaining $\hat{\beta}$

Application of fractal analysis on blood cell perfusion time series

Steps in the analysis used to obtain the fractal measures of the blood cell perfusion time series shown in Table 2 can be followed in the flowchart of Fig. 6. This flowchart is a guideline for analyzing one-dimensional physiological signals for potential characterization as a fractal, and uses the results of the numerical testing of the methods to designate a strategy for use on biological signals.

After taking a time series from a continuous temporal signal, one can decide whether the PSD exhibits power law behavior (similar to Eq. 1) over two decades of frequencies: the signal may be fractal. If it is not, alternatives such as the signal being periodic or chaotic can be explored.

Using $^{low}PSD_{w,e}$ and our SSC method we found that all of the blood cell perfusion time series were of the fBm type (Table 2). Our analysis yielded $\hat{H}^{fBM}_{bdSWV}$= 0.24±0.02 (n=8) for the physiological time series evaluated in this study.

Discussion

What we have learned from this study is that physiological time series can be analyzed with some assurance by carefully controlled fractal methods, and that the results are then meaningful. When series have adequate length (explored in detail in [5, 8, 9]) one can get nicely reproducible estimates of the correlation structure of the series, characterized by a single estimate of *H* when the signal is fractal. Knowing whether a signal is fractal, pe-

riodic or chaotic increases to our ability to determine the physiological basis of the signal.

Interpretation of fractal estimates obtained for physiological signals

If a signal, X_i, is found to be fractal with $H<0.5$, it exhibits long memory, that is, a correlation between its successive events whose decay over time is slower than $1/i$ [7]. Interpretation of fractal signals based on analyzing correlation structure is straightforward for fGn signals: they are positively correlated or anticorrelated, or fall into the special case of white or uncorrelated random noise (Fig. 2). As seen, fBm signals, including random walk, are all correlated with $r_1 \rightarrow 1$ as time approaches infinity. The question arises as to whether short-term and long-term trends can be present simultaneously in a motion signal, like our blood cell perfusion time series. If so, how can they be separated in our analysis? The ideal fBm signals on the left in Fig. 2 appear to have a smooth long-term component independent of H (take into account that, as t grows, it exceeds the window size of the panel Fig. 2), while the noise-like trends are more apparent with lower H values. Equation 2 shows that correlation in fBm signals depends on t, τ and H. The dependence on t defines the long-term positive correlation in the fBm signal but may not be what is physiologically meaningful; for example, in normal Brownian motion it only means that the increment during a time step is small compared with the displacement from the origin after a long time. However, correlation between *increments* of an fBm signal (Eq. 2) is informative and especially so when it is *independent* of t. The key in separating short- and long-term components in the fBm signal is using Eq. 2 on the raw and then on the differenced signal. Consequently, for the blood cell perfusion signals, the nearest neighbor correlation coefficient r_1 calculated by Eq. 2 or from $\hat{H}^{\mathrm{fBM}}_{\mathrm{bdSWV}}$ using Eq. 4 in this case indicates *anti-correlation* between *increments* of the fBm signal, because $\hat{H}^{\mathrm{fBM}}_{\mathrm{bdSWV}} = 0.24 \pm 0.02$ corresponds to $r_1 = -0.31 \pm 0.02$. The analysis method, bdSWV, by using SD for local statistics for obtaining $\hat{H}^{\mathrm{fBM}}_{\mathrm{bdSWV}}$, effectively deals with the non-stationary motion signal as if it were stationary. Therefore, $\hat{H}^{\mathrm{fBM}}_{\mathrm{bdSWV}}$ defines a short-term correlation structure in the fBm signal which is negative for the blood cell perfusion time series from the brain cortex of anesthetized rats: these series are fractal anticorrelated motion processes.

The catchment volume for the laser-Doppler probe includes many small vessels, arterioles and venules as well as capillaries. Why should the signal be fractal, and why should it not simply be random and uncorrelated noise with $H=0.5$? Why should it behave as a motion with anticorrelated increments? One possibility is that the power relationship might emanate from a vascular system in which a random signal with long memory (fractal regional blood cell perfusion in the brain cortex) is being produced from a number of highly focal (short-memory) blood cell perfusion time series resulting from the vasomotion activity of individual segments of the supplying vascular tree. The theoretical possibility for the generation of a macro-level long-memory fractal signal from a number of micro-level short-memory time series by aggregation has been shown by Granger [17]. One might therefore look for the basis on which such short-memory fluctuations in blood cell perfusion at the microregional level can produce a composite, fractally structured signal at the regional level by spatial integration.

There are perhaps two main possibilities for local anticorrelation in flow velocities. One is that arterioles and venules are both found in the same catchment region and can be expected to flow in opposite directions. The signal comes principally from erythrocytes, not vessel walls or other relatively stable tissue components. If one could obtain a signal from fluctuations from a single arteriole–venule pair, because red blood cell densities fluctuate continuously in both vessels, one would expect that a locally spatially integrated signal would exhibit anticorrelated behavior. In a spatially heterogeneous network of vessels most of the directional information is lost, leaving only relatively small local net fluctuations; these fluctuations are small relative to the total signal intensity. The other possibility is that neighboring arterioles fed by the same parent artery might fluctuate out of phase, one increasing flow at the transient expense of the other. This "local steal" would presumably be at much lower frequencies than those caused by red blood cell density fluctuations.

Neither really explains the characterization of the signal as a correlated fractional Brownian motion. At $\beta>1$ the signal's power is dominated by low frequencies. This is probably because, at low frequencies, slow fluctuations in pCO_2, pH, blood pressure or cardiac output govern the physiological regulation of the local state of vasodilatation and blood volume content. In contrast, high-frequency events, e.g., those mediated through local shear stress and nitric oxide (NO) release, are small, tend to be averaged out, and contribute less power to the signal.

Evaluating the methods and strategy for analysis

The principle of using signal conversion in the fractal analysis of physiological signals was based on using all of the features of the dichotomous fGn/fBm model. This model has the outstanding virtue of minimizing the number of parameters needed to describe a time series. More complex models, like the ARMA and ARIMA models, may provide useful detail but may not reveal the fundamental simplicity of the system. The fractional ARIMA, fARIMA, methods do allow the estimation of a non-integer exponent that characterizes the long memory component of a signal, and ought to be compared with our methods for efficiency and accuracy.

Viewing the time series through the simple fGn/fBm dichotomy did not yield a very simple method, although it is true that it can be completely automated. Our analyt-

ical strategy is summarized in a flowchart (Fig. 6), which we now follow.

Generating time series from the recorded physiological signal

A time series is defined as a set of discrete data points created by sampling a continuous signal at constant intervals Δt (Fig. 3). From the standpoint of the analyses presented in this paper, which are aimed at defining scaling properties, the value of Δt is immaterial. The time scale gains importance with respect to N, the length of the series, only when over- or undersampling is to be avoided. The sampling rate chosen has to be sufficiently high to avoid contamination the spectra by aliasing: specifically, at half of the sampling frequency (the Nyquist frequency) the power ought to become close to zero [25]. In principle a fractal signal will always become aliased since it contains infinite frequencies, but since the power diminishes with f steeply at high values of β, the power aliased rapidly becomes inconsequential. For our blood cell perfusion time series, this condition was met by sampling at 200 Hz.

The wide range of frequencies covered was essential to the analysis. Each series had $N=2^{17}$ or 131,072 points. Series length greatly influences both the bias and the variance of $\hat{H}$ [2, 5, 6, 8, 9, 29]. For example, to distinguish with probability $P<0.01$ between exact fractal Brownian motion series whose true H values differ by 0.1, series with at least 2^{15} (32,768) points are needed [9]. Our large N allowed finer distinction of DHM-generated signals, but this does not prove that biological series can be distinguished so well.

Are scaling properties in spectral estimates likely to be present?

For ideal (mathematical) fractals the range over which there is self-similarity is infinite. For biological fractals the range is restricted, by observation time and by the physical nature of the processes. One would like to see similarity over at least two decades of frequency to feel confident in using fractal approaches. The first decisive step in Fig. 6 is whether or not there is power-law scaling of adequate range.

The spectra for pure fGn or fBm signals are, however, only approximated by power law functions (Eq. 1), and the approximation is good only for low frequencies [7]. The reason for this is that when a regression line is fitted through $\log |A|^2$ versus $\log f$ using all frequencies, about the half of the spectral estimates in fact deviates from the nominal $1/f^{\beta}$ for the $1/2^3<f<1/2^1$ frequency range of the true spectra for both fGn and fBm signals ([7], see Fig. 2.5)]).

Hence, the scaling properties should only use low-frequency spectral densities for fitting the regression to obtain the slope β, as implemented by the ${}^{\text{low}}\text{PSD}_{\text{w,e}}$ method (between $1/2^N$ and $1/2^3$). In our blood cell perfusion time series ts.6, as seen in the PSD plot of Fig. 3, the scaling properties are present and extend over an almost four decade range whose upper limit is 25 Hz. Where a broad band PSD function is found, one with multiple peaks, the series should be rejected as being not fractal and considered as a chaotic process (Fig. 6).

Signal classification according to the dichotomous fGn/fBm model

Failure to match signal class with the appropriate method of fractal analysis results in serious error in estimating H. In the early [15] and even in more recent [28] applications of the fractal theory to the analysis of physiological time series, the importance of this issue was not clearly recognized. In contrast with our $\hat{H}^{\text{fBM}}_{\text{bdSWV}}=0.24\pm0.02$ for blood cell perfusion time series, Glenny et al. [15] reported an analysis of arteriolar red blood cell velocity fluctuations in rabbit tenuissimus muscle by Kislyakov et al. [21] giving $\hat{H}_{\text{Disp}}=0.84$ and Rossitti et al. [28] found $\hat{H}_{\text{Disp}}=0.76$ for axial blood flow velocity in the middle cerebral artery in man. Both used dispersional analysis, which should only be used for fGn. When dispersional analysis is applied to our blood cell perfusion time series, now known to be an fBm with H about 0.24, the result gives an erroneous estimated $\hat{H}$ of 0.89. The inference is that estimates of H reported by Glenny et al. [15] and Rossitti et al. [28] are probably wrong and that the true signals might be fBm's with H near 0.2 rather than fGn's. Their series were too short to allow precise evaluation so we cannot know the answer.

Perhaps the central importance of signal classification in fractal analysis has not been recognized sooner because the distinction between fractal noise and fractal motion was not recognized as being needed to interpret the physiology.

Using stationary and non-stationary random signal categories, fGn and fBm, is likely to cover most signals. But fractals exist with $\beta>3$; their 2nd or 3rd, etc. differences or increments are stationary. They would fall into the category of stochastic fractals too. Statistically, fGn and fBm are simple models each with just two parameters, a variance and the low-frequency scaling parameter, H. A more comprehensive class of models that have the same low-frequency properties as fGn and fBm is the class of fractional ARIMA (fARIMA) models [7]. With only two parameters, it is not possible to model the high-frequency structure that would distinguish fGn and fBm from the fARIMA models, which will have more parameters. However, most signals in physiology are dominated by their low frequencies, like the blood cell perfusion signals evaluated in this study. Hence, we believe that fractal analysis has general applicability in physiology, and also that sophisticated models, like fARIMA, should be considered.

Signal classification should begin with ${}^{\text{low}}\text{PSD}_{\text{w,e}}$, since it can be applied to both fGn and fBm. But this

method does not find the true β in the range of $0.38<\beta<1.04$ very well (see Figs. 4 and 5) because of its marked bias in the range of $0<H<0.1$ which results in false estimates of β both in terms of value and class. Our SSC method narrows the range of uncertainty of ${}^{low}PSD_{w,e}$ by supplementing it with further analysis with bdSWV around the critical fGn/fBm boundary (Fig. 4 C2). Incorporating the step of summation makes bdSWV applicable to both fGn and fBm signals. Because of its bias in estimating $\hat{H}$' for summed motion signals in the low range of H, it has its own range of uncertainty, too. If $\hat{\beta}$ calculated from $\hat{H}$' falls in the range $0.6<\beta<1$ the analysis via our dichotomous strategy is weak, as seen by the high misclassification rate in Fig. 5, bottom right panel. Notice that ${}^{low}PSD_{w,e}$ and our SSC method found the correct signal category, fBm, for all blood cell perfusion time series (Table 2) because $\hat{\beta}$ values given by these methods fell in the range where the misclassification rate is 0% (Fig. 5). For these data, one could say that the SSC method was not needed to arrive at the correct signal class, but that it also provided more security in the estimation of H.

Estimating *H*

Selection of the best tools that can be applied to physiological signals with a reasonably high expectation of providing a reliable estimate of H is a difficult task to complete. Our numerical experiments (Fig. 4) have shown that the methods appear to be biased and have variance in their estimate around the true H. The exception to this is the specific case when the method shares the same basis for signal generation and analysis, such as ${}^{low}PSD_{w,e}$. We used two robust tools, Disp for fGn and bdSWV for fBm signals, whose estimates of H were independent of the algorithm for the process producing the signal. Disp and bdSWV demonstrated very low MSE's of 0.00056 and 0.00006 for $0.1<H<0.9$ (Fig. 4), and thus proved to be excellent estimators of H.

The inconsistencies of the periodogram method may stem partly from the fact that in Eq. 1 the left- and the right-hand sides are not really equal, but relate to each other in an approximate manner, one representing a sample statistic, the other a population quantity. Without an expectation operation, the left-hand side fails to converge to the right-hand side (no matter how much data are taken) – one has to do something to the left-hand side (smoothing, regression fits, or averaging) to get a reasonable spectral estimate [20]. In extensive numerical testing, we found that ${}^{low}PSD_{w,e}$ gives the best overall performance of the various spectral techniques, which demonstrates the importance of the expectation operations in making PSD a reliable tool to be applied to physiological signals too.

Spectral methods are sensitive to high-frequency disturbances, as mentioned above, while Disp and bdSWV are not, because they bin these frequencies into one point. Even when high-frequency biasing of $\hat{\beta}$ from ${}^{low}PSD_{w,e}$ is minimized by omitting the upper half of the spectrum from the regression, the MSE of $\hat{\beta}$ is still two magnitudes higher than that of bdSWV, and one magnitude higher than that of Disp (Fig. 4).

For Disp, and bdSWV, there are few points in the regression fit as compared to the spectral methods. Each point in Disp and bdSWV can be taken to be (roughly) the equivalent to the average of a group of spectral ordinates. Because the basic Disp and bdSWV points have inherently less variability, the correlation coefficient of the power-law fit for these methods will be higher than that for the spectral methods; however, this does not necessarily translate into a better fractal estimate. Since each Disp and bdSWV point is highly smoothed, whereas each spectral ordinate is not, it is natural that r would be higher for these methods than for the spectral methods.

Raymond and Bassingthwaighte [27] showed that Disp and SWV methods both derive their effectiveness by eliciting the degree of long memory correlation in the signal. Using the terminology of Caccia et al. [8], both of these methods use three statistical measures: local, partition-based and transscale. They are implemented in a hierarchical order: for Disp the order is the local mean, the SD of all the means, then H. For SWV it is the local SD, the mean of the SD's, then H. Disp is specific for fGn. SWV calculates H on a non-stationary fBm signal by using SD for local statistics. The power law growth of the SD with τ gives the direct measure of H.

Acknowledgements A computer program "Fractool" running on the Macintosh, PC, and Unix platforms written by the authors for estimating the Hurst coefficient of physiological time series are available on the Web at http://www.elet2.sote.hu/eke/FRACTPHYS/. This program can be freely distributed as long as the "readme" file is included and the use of the program is properly acknowledged. The authors thank Professor Peter Sandor for lending his LDF monitor, and Professor Dick Slaaf, Maastricht University, for his insightful critiques of the manuscript. Supported by OTKA Grants I/3 2040, E 012235, T 016953 and NIH Grant TW00442.

References

1. Bassingthwaighte JB (1988) Physiological heterogeneity: fractals link determinism and randomness in structures and function. News Physiol Sci 3:5–10
2. Bassingthwaighte JB, Beard DA, Percival DB, Raymond GM (1995) Fractal structures and processes. Workshop on chaos and fractals. Mobile, Alabama. American Institute of Physics, One Physics Elliipse, College Park, Maryland 20740-3743
3. Bassingthwaighte JB, Beyer RP (1991) Fractal correlation in heterogeneous systems. Physica D 53:71–84
4. Bassingthwaighte JB, Liebovitch LS, West BJ (1994) Fractal physiology. Oxford University Press, New York
5. Bassingthwaighte JB, Raymond GM (1994) Evaluating rescaled range analysis for time series. Ann Biomed Eng 22: 432–444
6. Bassingthwaighte JB, Raymond GM (1995) Evaluation of the dispersional analysis method for fractal time series. Ann Biomed Eng 23:491–505
7. Beran J (1994) Statistics for long-memory processes. Chapman and Hall, New York
8. Caccia DC, Percival DB, Cannon MJ, Raymond GM, Bassingthwaighte JB (1997) Analyzing exact fractal time se-

ries. Evaluating dispersional analysis and rescaled range methods. Physica A 246:609–632
9. Cannon MJ, Percival DB, Caccia DC, Raymond GM, Bassingthwaighte JB (1997) Evaluating scaled window variance methods for estimating the Hurst coefficient of time series. Physica A 241:606–626
10. Cavalcanti S, Ursino M (1996) Chaotic oscillations in microvessel arterial networks. Ann Biomed Eng 24:34–47
11. Davies RB, Harte DS (1987) Test for Hurst effect. Biometrika 74:95–101
12. Diggle PJ (1990) Time series: a biostatistical introduction. Oxford Science, Oxford
13. Eke A, Herman P, Bassingthwaighte JB, Raymond GM, Cannon M, Balla I, Ikrenyi C (1997) Temporal fluctuations in regional red blood cell flux in the rat brain cortex is a fractal process. Adv Exp Med Biol 428:703–709
14. Fougere PF (1985) On the accuracy of spectrum analysis of red noise processes using maximum entropy and periodogram methods: simulation studies and application to geographical data. J Geograph Res 90(A5):4355–4366
15. Glenny RW, Robertson HT, Yamashiro S, Bassingthwaighte JB (1991) Applications of fractal analysis to physiology. J Appl Physiol 70:2351–2367
16. Goldberger AL, West BJ (1987) Fractals in physiology and medicine. Yale J Biol Med 60:421–435
17. Granger CWJ (1980) Long memory relationships and the aggregation of dynamic models. J Econometrics 14:227–238
18. Griffith TM, Edwards DH (1993) Mechanism underlying chaotic vasomotion in isolated resistance arteries: roles of calcium and EDRF. Biorheology 30:333–347
19. Hurst HE (1951) Long-term storage capacity of reservoirs. Trans Am Soc Civil Eng 116:770–808
20. Jenkins GM, Watts DG (1968) Spectral analysis and its applications. Holden-Day, San Francisco
21. Kislyakov Y, Levkovitch Y, Shuymilova T, Vershinina E (1987) Blood flow fluctuations in cerebral cortex microvessels. Int J Microcirc Clin Exp 6:3–13
22. Mandelbrot BB (1983) The fractal geometry of nature. WH Freeman, San Francisco
23. Mandelbrot BB (1985) Self-affine fractals and fractal dimension. Phys Sci 32:257–260
24. Mandelbrot BB, van Ness JW (1968) Fractional brownian motions, fractional noises and applications. SIAM Rev 10:422–437
25. Pandit SM (1991) Model and spectral analysis: data dependent systems in state space. John Wiley, New York
26. Peng CK, Buldyrev SV, Havlin S, Simons M, Stanley HE, Goldberger AL (1994) Mosaic organization of DNA nucleotides. Phys Rev E 49:1685–1689
27. Raymond GM, Bassingthwaighte JB (1999) Deriving dispersion and scaled windowed variance fractal analyses using the correlation function of discrete fractional Gaussian noise. Physica A 265:85–96
28. Rossitti S, Stephensen H (1994) Temporal heterogeneity of the blood flow velocity at the middle cerebral artery in the normal human characterized by fractal analysis. Acta Physiol Scand 151:191–198
29. Saupe D (1988) Algorithms for random fractals. In: Peitgen HO, Saupe D (eds) The science of fractal images. Springer, Berlin Heidelberg New York, pp 71–136
30. Schepers HE, van Beek JHGM, Bassingthwaighte JB (1992) Four methods to estimate the fractal dimension from self-affine signals. IEEE Eng Med Biol 11:57–71
31. Schmittbuhl J, Violette JP, Roux S (1995) Reliability of self-affine measurements. Phys Rev E 51:131–147
32. Schuster A (1898) On the investigation of hidden periodicities with application to a supposed 26 day period of meteorological phenomena. J Geophys Res 3:13–41
33. Slaaf DW, Yamashiro SM, Tangelder GJ, Reneman RS, Bassingthwaighte JB (1993) Nonlinear dynamics of vasomotion. In: Allegra C, Intaglietta M, Messmer K (eds) Vasomotion and flowmotion. Karger, Basel, pp 67–80
34. Turcott RG, Teich MC (1995) Interevent-interval and counting statistics of the human heartbeat for heart-failure and normal patients. Ann Biomed Eng 24:269–293
35. Van Beek JGHM, Roger SA, Bassingthwaighte JB (1989) Regional blood flow heterogeneity explained with fractal networks. Am J Physiol 257:H1670–H1680
36. Voss RF (1988) Fractals in nature: from characterization to simulation. In: Peitgen HO, Saupe D (eds) The science of fractal images. Springer, Berlin Heidelberg New York, pp 21–70
37. Weibel ER (1991) Fractal geometry: a design principle for living organisms. Am J Physiol 261:L361–L369